First-Principles Nonadiabatic Dynamics of Molecules at Metal Surfaces with Vibrationally Coupled Electron Transfer

Gang Meng[1], James Gardner[2], Nils Hertl[2], Wenjie Dou[3], Reinhard J. Maurer[2,4,*] and Bin Jiang[1,5,†]

[1]Key Laboratory of Precision and Intelligent Chemistry, Department of Chemical Physics, University of Science and Technology of China, Hefei, Anhui, China

[2]Department of Chemistry, University of Warwick, Coventry CV4 7AL, United Kingdom

[3]Department of Chemistry, School of Science, Westlake University, Hangzhou 310024 Zhejiang, China

[4]Department of Physics, University of Warwick, Coventry CV4 7AL, United Kingdom

[5]Hefei National Laboratory, University of Science and Technology of China, Hefei, 230088, China

(Received 4 January 2024; accepted 12 June 2024; published 19 July 2024)

Accurate description of nonadiabatic dynamics of molecules at metal surfaces involving electron transfer has been a long-standing challenge for theory. Here, we tackle this problem by first constructing high-dimensional neural network diabatic potentials including state crossings determined by constrained density functional theory, then applying mixed quantum-classical surface hopping simulations to evolve coupled electron-nuclear motion. Our approach accurately describes the nonadiabatic effects in CO scattering from Au(111) without empirical parameters and yields results agreeing well with experiments under various conditions for this benchmark system. We find that both adiabatic and nonadiabatic energy loss channels have important contributions to the vibrational relaxation of highly vibrationally excited CO($v_i = 17$), whereas relaxation of low vibrationally excited states of CO($v_i = 2$) is weak and dominated by nonadiabatic energy loss. The presented approach paves the way for accurate first-principles simulations of electron transfer mediated nonadiabatic dynamics at metal surfaces.

DOI: 10.1103/PhysRevLett.133.036203

Energy transfer during gas-surface collisions plays a crucial role in many interfacial phenomena [1]. Various degrees of freedom (DOF)—molecular vibration, rotation, and translation, along with surface phonons and electrons—can potentially couple to each other, leading to intricate energy transfer dynamics. Especially at metal surfaces, the energy threshold for electronic excitations in metals is infinitesimally small rendering nonadiabatic energy exchange between molecular motion and metallic electrons inevitable. Experiments of adsorbate vibrational lifetimes [2], chemicurrents [3], and hydrogen atom scattering [4] have provided clear evidence of nonadiabatic effects at metal surfaces. These effects have been largely understood by electronic friction (EF) based models [5,6], in which weak nonadiabatic energy dissipation is treated perturbatively [4,7–11].

In contrast, the scattering of vibrationally excited NO and CO molecules from metal surfaces manifests diverse vibrational energy transfer effects that depend on molecule and substrate [12–15], the initial vibrational state [16,17], and the molecular orientation [16,18]. The observed multiquantum vibrational relaxation is associated with vibrationally enhanced electron transfer from metals to molecules [12]—a strong nonadiabatic effect involving the formation of a transient ionic state as qualitatively interpreted by low-dimensional phenomenological models [19]. Meanwhile, recent Born-Oppenheimer molecular dynamics (BOMD) studies based on first-principles machine-learned potential energy surfaces (PESs) indicate that vibrational energy may transfer efficiently to other low frequency modes, as the molecule approaches the dissociation barrier region [20–22]. On top of an adiabatic PES, MD simulations with EF (MDEF) based on density functional perturbation theory can capture the single-quantum and orientation-dependent vibrational relaxation in the scattering of NO($v_i = 3$) from Au(111) [23,24], but largely underestimate the multiquantum vibrational relaxation and overestimate molecular trapping for highly vibrationally excited NO [23].

To better describe these events, it is essential to accurately capture both the high-dimensional PES and nonadiabatic electronic transitions. Among methods for nonadiabatic dynamics near metal surfaces that go beyond the classical EF theory [25–28], the independent electron surface hopping (IESH) [25] approach is the most used one [29–31]. In addition, it is the only method that has thus far been invoked to describe the high-dimensional dynamics of a realistic system based on electronic structure theory, specifically for NO on Au(111), with some successes [25,32–34]. This method takes an independent electron representation and allows for single electron hopping within a manifold of electronic states that couple discretized metallic and molecular levels in a mixed quantum-classical manner. Unfortunately, it later turned out that the parametrization of diabatic states constructed with an

*Contact author: R.Maurer@warwick.ac.uk

†Contact author: bjiangch@ustc.edu.cn

effective perturbative approach based on an applied electric field failed to capture important features of the dynamics. This resulted in disagreements with experiments under various conditions [17,24,35].

We recently proposed a more general way to calculate charge-transfer states of molecules at metal surfaces by constrained density functional theory (CDFT), which successfully described the electron transfer behavior of NO and CO on different metal surfaces [36]. In this Letter, we use a high-dimensional machine-learning algorithm to represent CDFT energies for varied nuclear configurations for the construction of an effective diabatic Hamiltonian for IESH, enabling a first-principles description of nonadiabatic dynamics at metal surfaces mediated by electron transfer. As a proof of concept, we study the $CO + Au(111)$ system, in which the nonadiabatic effects are subtle and both adiabatic and nonadiabatic energy transfer channels need to be accurately captured [14,37].

The IESH method originates from a discretized version of the Newns–Anderson Hamiltonian [38] considering only two molecular electronic configurations, i.e., the neutral and negative ion states. In this model, the many-electron Hamiltonian is expressed as a sum of one-electron terms given by [25,31],

$$H(\mathbf{R},\mathbf{P}) = \sum_{i=1}^{3N} \frac{P_i^2}{2M_i} + U_0(\mathbf{R}) + \sum_{j\in \mathbf{s}(t)} E_j(\mathbf{R}), \quad (1)$$

where the first term is the nuclear kinetic energy and the third term is the sum of energies of occupied one-electron orbitals indexed in the time-dependent $\mathbf{s}$ vector. $E_j(\mathbf{R})$ is the jth orbital energy or the jth eigenvalue of the one-electron Hamiltonian,

$$H_{el}^1(\mathbf{R}) = (U_1(\mathbf{R}) - U_0(\mathbf{R}))|a\rangle\langle a| + \sum_{k=1}^{M} \varepsilon_k |k\rangle\langle k| + \sum_{k=1}^{M} V_{ak}(\mathbf{R})(|a\rangle\langle k| + |k\rangle\langle a|), \quad (2)$$

where $U_0(\mathbf{R})$ [or $U_1(\mathbf{R})$] represents the interaction potential between the metal surface and the neutral molecule (or the negative ion when the lowest unoccupied orbital of the molecule, $|a\rangle$, is occupied). The metallic continuum is discretized by M one-electron orbitals $\{|k\rangle\}$ corresponding to one-electron energies of $\{\varepsilon_k\}$. $V_{ak}(\mathbf{R})$ represents the coupling strength between $|a\rangle$ and $|k\rangle$, which is often assumed to be constant over the relevant energy range. In this representation, the ground state corresponds to filling the $N_e (N_e = M/2)$ lowest energy one-electron eigenstates up to the Fermi level, while excited states are produced by promoting one or more electrons to unoccupied states. One then employs the modified "fewest switches" surface hopping algorithm [39] to model transitions of multiple independent electrons [25]. More details of the IESH method are given in the Supplemental Material [40] (Figs. S1–S3).

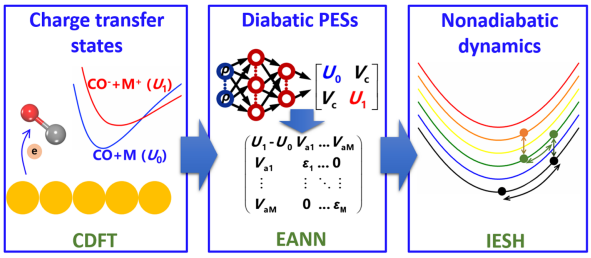

FIG. 1. Schematic workflow of nonadiabatic dynamics simulations of molecules (CO, for example) at metal surfaces involving electron transfer between them.

Here, we propose to parameterize the IESH Hamiltonian by the CDFT-based diabatic states and corresponding machine learning potentials as illustrated in Fig. 1. There are several critical improvements of this workflow over the initial IESH application to the $NO + Au(111)$ system [25,32,33]. First, $U_0(\mathbf{R})$ [or $U_1(\mathbf{R})$] is determined by CDFT, for which a net Bader charge of $0e$ or $-1e$ is constrained to the molecule by adjusting self-consistently an external potential in the modified Kohn-Sham equations [51,52]. As depicted in Fig. S4 [40], CDFT is more stable than the previous electric field-based perturbative method [32], ensuring better asymptotic behavior and global smoothness of diabatic states. Second, to overcome the failure of previously used empirical functions to describe molecular dissociation and anharmonicity of the lattice vibration [32], we utilize a high-fidelity embedded atom neural network (EANN) method [53,54] to learn CDFT energies, yielding high-dimensional diabatic PESs that are as accurate as the adiabatically ground state (E_g) PES learned from conventional DFT energies and forces. The off-diagonal coupling (V_c) between the two diabatic states can be derived by enforcing consistency between E_g and the lowest eigenvalue of the 2×2 diabatic Hamiltonian. V_c is then used to parametrize $V_{ak}(\mathbf{R})$ in Eq. (2) (see Supplemental Material [40]) [25]. Specifically, CDFT calculations for $CO + Au(111)$ were performed with CP2K [55] in a slab model of a 6×6 supercell with four metal layers using the Van der Waals density functional (vdW-DF) [56]—the same level of theory used for E_g [22]. As shown in Fig. 2, although U_1 is generally higher in energy than U_0 at most area, the two diabats do cross at very short molecular height and very long C-O distance, which plays an important role in nonadiabatic energy transfer. The EANN potentials nicely reproduce CDFT (and ground state DFT) energies, capturing the crossing between diabatic states. More details and the validation of ground and diabatic PESs are given in Supplemental Material [40] (Figs. S5–S6).

We apply this approach to study state-to-state scattering of CO from Au(111), where extensive experimental data

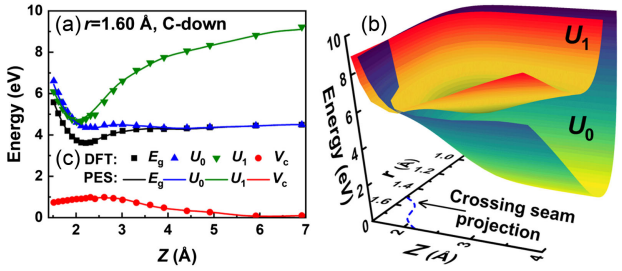

FIG. 2. (a) Potential energy curves of the ground state (E_g), the neutral (U_0), anionic state (U_1), and the diabatic coupling (V_c) as a function of the molecular height (Z) above Au(111). CO is perpendicular to the hcp site with a long bond distance ($r = 1.60$ Å) and C-down orientation. (b) Diabatic state PESs as a function of r and Z, where the crossing seam of the diabatic states is projected onto the r-Z plane (dashed line). The energy zero is E_g of the free CO molecule far from the surface.

exist [14,57,58]. First, Fig. 3 compares the final vibrational state distributions of highly vibrationally excited CO($v_i = 17$) scattered from Au(111) calculated by BOMD and IESH simulations, with experimental data at three translational incidence energies (E_i) [14]. The experimental survival probability of CO($v_i = 17$) decreases as E_i increases from 0.24 to 0.57 eV and the vibrational state relaxes down to $v_f = 14$. BOMD predicts the proper E_i dependence of vibrational relaxation, yet overestimates the survival probability by 0.1–0.2. The promoted vibrational energy loss for molecules at higher E_i is attributable to their higher accessibility to the dissociation barrier region where the molecular vibration softens and couples to translation [21,22]. In comparison, IESH predicts more significant vibrational relaxation and brings the calculated vibrational state distributions close to measured ones.

To elaborate different energy transfer pathways, Table I summarizes the mean energy loss (or gain) of molecular vibration ($\langle \Delta E_{vib} \rangle$), rotation ($\langle \Delta E_{rot} \rangle$), translation ($\langle \Delta E_{trans} \rangle$), surface phonons ($\langle \Delta E_{ph} \rangle$), and surface electrons ($\langle \Delta E_{el} \rangle$) during CO($v_i = 17$) scattering at $E_i = 0.57$ eV.

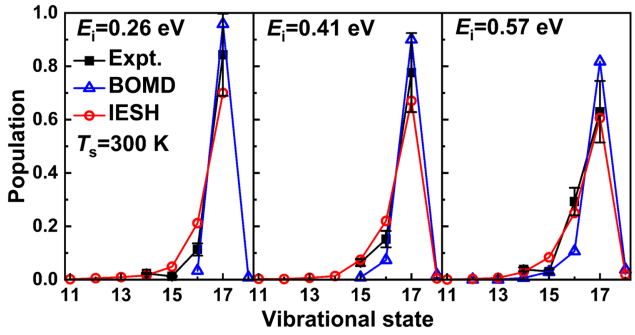

FIG. 3. Comparison of experimental final vibrational state distributions [14] of CO($v_i = 17$) scattered from Au(111) at different incidence energies with BOMD and IESH results based on the vdW-DF PES. The surface temperature (T_s) is 300 K, as in experiments.

BOMD results show that the translational energy of CO is largely transferred to rotation (~0.12 eV) and phonons (~0.24 eV) during vibrationally elastic scattering. In comparison, for vibrationally inelastic scattering, $\langle \Delta E_{trans} \rangle$ is greatly increased by ~0.18 eV that well matches the vibrational energy loss, implying that vibration is mainly coupled to translation in this process. Experiments have also indicated a certain degree of vibration-to-translation coupling in NO scattering from Au(111) [59]. Interestingly, IESH simulations barely change the energy exchange among other DOF, except that $\langle \Delta E_{trans} \rangle$ is now ~0.11 eV lower than that in BOMD for vibrationally inelastic scattering. On average, vibrational energy is primarily transferred to surface electrons (~0.19 eV), secondarily to translation (~0.09 eV), while negligibly to rotation and surface phonons. Comparison of representative trajectories of BOMD and IESH with identical initial conditions in Fig. S7 [40] clearly shows that the energy variation in translation, rotation, and surface phonons is hardly affected by considering energy dissipation due to electronic excitation. In turn, the lattice motion has little influence on vibrational energy transfer in BOMD and IESH simulations (Fig. S8 [40]). These results indicate that, under these conditions and for this system, the adiabatic and nonadiabatic pathways of vibrational energy transfer are rather independent and both represent additive contributions. The latter always dominates but the former cannot be neglected. The IESH trajectory in Fig. S7 [40] also shows that the vibrational to electronic energy transfer likely occurs as the molecule gets close to the surface (2–3 Å) and the nonadiabatic coupling becomes strong. Meanwhile, the molecule quickly bounces back due to the short-range repulsion so that this nonadiabatic energy transfer process is ultrafast (<100 fs) at a high E_i. Importantly, this abrupt electronic transition may stride across several one-electron states at one time, leading to an immediate increment of electronic energy. This picture is different from that of the Markovian EF model, in which the vibrational energy is progressively dissipated to an electronic bath through a frictional force.

TABLE I. Average vibrational, rotational, translational, surface phonon, and surface electron energy losses (or gains) (in eV) of CO($v_i = 17, E_i = 0.57$ eV) scattering from Au(111) in BOMD and IESH simulations. Vibrationally elastic ($v_f = 17$) and inelastic ($v_f \neq 17$) channels are separately listed.

Mean energy change (eV)	BOMD		IESH	
	$v_f = 17$	$v_f \neq 17$	$v_f = 17$	$v_f \neq 17$
$\langle \Delta E_{vib} \rangle$	−0.01	−0.17	−0.01	−0.28
$\langle \Delta E_{rot} \rangle$	0.12	0.07	0.13	0.09
$\langle \Delta E_{trans} \rangle$	−0.35	−0.17	−0.36	−0.28
$\langle \Delta E_{ph} \rangle$	0.24	0.27	0.24	0.28
$\langle \Delta E_{el} \rangle$	0.00	0.00	0.00	0.19

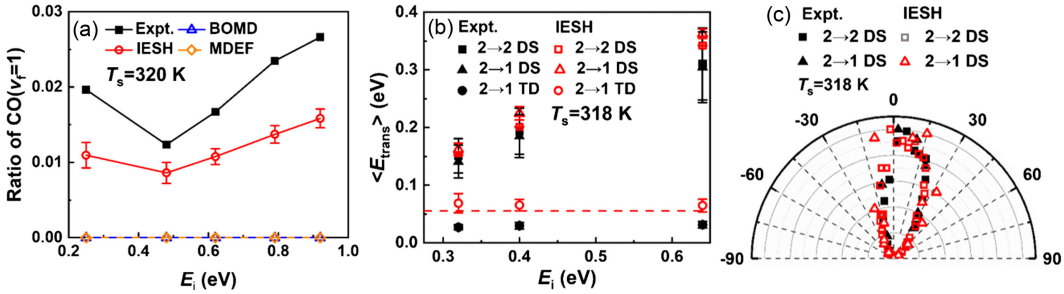

FIG. 4. Comparison of various experimental [57,58] and calculated results on the vdW-DF PES for the scattering of CO($v_i = 2$) from Au(111), including (a) product branching ratio of CO($v_f = 1$) and (b) final mean translational energy ($\langle E_{trans} \rangle$) of different channels as a function of E_i, and (c) angular distributions for vibrationally elastic ($2 \rightarrow 2$) and inelastic ($2 \rightarrow 1$) channels of the DS component at $E_i = 0.32$ eV. Red dashed line in panel (b) indicates the thermal limit, i.e., $\langle E_{trans} \rangle = 2k_b T_s$. Error bars reflect standard errors due to finite trajectories at each condition.

Next, we focus on the scattering of CO in a low vibrational state ($v_i = 2$) from Au(111), which represents a benchmark process that exhibits weak nonadiabaticity [57,58]. As shown in Fig. 4(a), the vibrational inelasticity of CO($v_i = 2$) is much weaker than that of CO($v_i = 17$). Moreover, the vibrational relaxation probability first decreases and then increases with increasing E_i. Notably, BOMD results fail to predict any vibrational inelasticity. In contrast, present IESH results reproduce the small but finite relaxation probability for CO($v_i = 2 \rightarrow v_f = 1$) within a factor of 2 compared to experiments and its E_i dependence. This signifies that the vibrational motion of CO($v_i = 2$) couples solely, albeit weakly, to surface electrons, which is essential to trigger the vibrational relaxation. Indeed, molecules in this lower state cannot access the dissociation region so that the adiabatic vibration-to-translation coupling becomes negligible. Importantly, we find that vibrational relaxation arises mostly from direct scattering (DS) trajectories for 0.48 eV $\leq E_i \leq$ 0.92 eV. In this range, the increasing incidence energy renders the molecule closer to the strong coupling region near the surface resulting in more facile electron hopping. While at $E_i = 0.25$ eV, which is close to the physisorption well depth of CO on Au(111) (0.19 eV), around 60% of inelastic CO($v_f = 1$) products are resulted from those trajectories being temporarily trapped before desorption (TD) and experiencing an increased chance of electron hopping. Figure S9 [40] demonstrates the representative DS and TD trajectories with fast and slow electron hopping, respectively. Additionally, it is found that the positions for occurring electron hopping are generally farther from the surface at $E_i = 0.25$ than at $E_i = 0.92$ eV, and dominated by the TD component near the physisorption well. This higher TD contribution facilitates the vibrational coupling to surface electrons, thereby explaining the increased relaxation probability at $E_i = 0.25$ eV. Interestingly, MDEF calculations based on the friction tensor derived from the present Newns-Anderson Hamiltonian in the wide band limit [34] yield near-zero vibrational relaxation probabilities at both high and low E_i [see Fig. 4(a)], suggesting that the nonadiabatic effects in CO($v_i = 2$) scattering are largely nonperturbative and thus not interpretable by the Markovian EF theory.

The IESH results also agree with experimental data of mean translational energy ($\langle E_{trans} \rangle$) and angular distributions of scattered CO molecules [57], as shown in Figs. 4(b)–4(c). Specifically, CO($v_f = 2$) and CO($v_f = 1$) molecules obtained from the DS channel have very close $\langle \Delta E_{trans} \rangle$, both of which increase linearly with E_i. This indicates some memory of their initial conditions and confirms that vibrational energy loss to translation is negligible. They also share similarly narrow scattering angular distributions peaking near the specular angle, as expected for a DS process. By contrast, the $\langle E_{trans} \rangle$ of the TD component of CO($v_f = 1$) is much smaller and close to the thermal limit, i.e., $2k_b T_s$, where T_s is the surface temperature of 318 K. It is nearly independent of E_i, suggesting that these molecules are largely equilibrated with the surface before desorption. Quantitatively, the calculated $\langle E_{trans} \rangle$ of CO($v_f = 1$) molecules in the TD channel is slightly higher than the thermal limit as trapped trajectories are identified here by the maximum simulation time (50 ps), where thermalization may be incomplete.

Finally, Fig. S10 [40] shows that previous BOMD results [22] using an alternate PES based on the BEEF-vdW functional [37], which gives a dissociation barrier that is ~0.5 eV lower than the vdW-DF PES, heavily overestimate vibrational relaxation for CO($v_i = 17$) compared to experiments. One would expect even larger discrepancy with experiments using this PES if nonadiabatic effects were accounted for. By contrast, this BEEF-vdW PES predicts negligible vibrational relaxation probabilities ($\sim 10^{-4}$) for CO($v_i = 2$) when simulated with BOMD and with MDEF within the local density approximation [37], in qualitative disagreement with experiments (see Fig. S11 [40] and Ref. [37]). This indicates that vibrational energy transfer is quite sensitive to the precise energy landscape in the barrier region, which is a crucial prerequisite for the correct nonperturbative treatment of electron transfer mediated nonadiabatic dynamics.

To summarize, we propose a novel computational scheme to enable a first-principles description of electron transfer-mediated nonadiabatic dynamics for molecules weakly or moderately bonded with metal surfaces, which have been extensively studied in experiments [12–15,57,60]. In this scheme, charge-transfer states are determined by CDFT and full-dimensional diabatic PESs are represented by EANN, which are then integrated with the IESH algorithm allowing for energy flow to both surface phonons and electrons. Taking the $CO + Au(111)$ system as an example, the simulation results achieve best agreement so far with experiments for both $CO(v_i = 17)$ and $CO(v_i = 2)$ scattering events from Au(111). Moreover, it is found that in the case of $CO(v_i = 17)$, vibration is predominantly coupled nonadiabatically to surface electrons, followed by adiabatic coupling to translation. While in the case of $CO(v_i = 2)$, vibration becomes almost exclusively coupled to surface electrons so that BOMD is unable to predict any vibrational inelasticity. Note that the present finding does not conflict with the previously proposed adiabatic energy transfer mechanism for $NO/Au(111)$ and $CO/Au(111)$ that relates to the ability of the molecule reaching the dissociation barrier [21,22,61]. Since this barrier is much lower for NO than for CO on Au(111), the adiabatic channel is less important in the latter case where the nonadiabatic channel dominates. This is particularly true for $CO(v_i = 2)$, as the molecule is almost unable to access the barrier.

This work introduces new opportunities for studying high-dimensional nonadiabatic dynamics at metal surfaces. As a starting point, the CDFT-based diabatic state PESs can be integrated with other nonadiabatic dynamical methods such as the (broadened) classical master equation (BCME) [27]. Admittedly, the CDFT method may work less well for strongly bound systems, where charge transfer states are not easy to be clearly defined. In such scenarios, however, explicit charge transfer states may be unnecessary and an EF-based description could work well [62,63]. The IESH approach, similar to other surface hopping approaches, is known to suffer from overcoherence effects in the dynamics. Recently, a decoherence correction was applied to IESH [64], which was shown to yield a minor effect on nonadiabatic energy loss for NO scattering on Au(111) and Ag(111). Recent progresses have also been made on quantizing the molecular vibration [65] in IESH and an alternative linearized semi-classical method [66], both limited to two-dimensional models. Unfortunately, accurate nonadiabatic quantum dynamical simulations in realistic systems are still lacking. Further work is necessary to conclude whether the parametrization of the Hamiltonian or the dynamical method is more critical to achieving quantitative accuracy. A more comprehensive comparison of various mixed quantum-classical nonadiabatic dynamical theories using the same parametrized high-dimensional Hamiltonian will be highly valuable in this regard.

The reported diabatic and coupling PESs, as well as the CDFT dataset are freely available from the GitHub repository [67]. Nonadiabatic dynamics simulations could be reproduced by the NQCDynamics.jl code [68], as has been previously released at [69].

Acknowledgments—This work is supported by the Strategic Priority Research Program of the Chinese Academy of Sciences (XDB0450101), Innovation Program for Quantum Science and Technology (2021ZD0303301), National Natural Science Foundation of China (22325304 and 22221003), CAS Project for Young Scientists in Basic Research (YSBR-005), the Leverhulme Trust (RPG-2019-078), the UKRI Future Leaders Fellowship program (MR/X023109/1), and a UKRI Frontier research grant (EP/X014088/1). Calculations have been done on the supercomputing center of USTC and Hefei Advanced Computing Center. We thank Alec Wodtke, Dan Auerbach, Tim Schäfer, Igor Rahinov, Kai Golibrzuch, Pranav R. Shirhatti, John Tully, and Hua Guo for helpful discussions.

[1] G. B. Park, B. C. Krüger, D. Borodin, T. N. Kitsopoulos, and A. M. Wodtke, Rep. Prog. Phys. **82**, 096401 (2019).
[2] M. Morin, N. J. Levinos, and A. L. Harris, J. Chem. Phys. **96**, 3950 (1992).
[3] B. Gergen, H. Nienhaus, W. H. Weinberg, and E. W. McFarland, Science **294**, 2521 (2001).
[4] O. Bünermann, H. Jiang, Y. Dorenkamp, A. Kandratsenka, S. M. Janke, D. J. Auerbach, and A. M. Wodtke, Science **350**, 1346 (2015).
[5] M. Head-Gordon and J. C. Tully, J. Chem. Phys. **103**, 10137 (1995).
[6] J. I. Juaristi, M. Alducin, R. Díez Muiño, H. F. Busnengo, and A. Salin, Phys. Rev. Lett. **100**, 116102 (2008).
[7] A. Kandratsenka, H. Jiang, Y. Dorenkamp, S. M. Janke, M. Kammler, A. M. Wodtke, and O. Bünermann, Proc. Natl. Acad. Sci. U.S.A. **115**, 680 (2018).
[8] S. P. Rittmeyer, J. Meyer, J. I. Juaristi, and K. Reuter, Phys. Rev. Lett. **115**, 046102 (2015).
[9] M. Askerka, R. J. Maurer, V. S. Batista, and J. C. Tully, Phys. Rev. Lett. **116**, 217601 (2016).
[10] M. Blanco-Rey, J. I. Juaristi, R. Díez Muiño, H. F. Busnengo, G. J. Kroes, and M. Alducin, Phys. Rev. Lett. **112**, 103203 (2014).
[11] D. Novko, J. C. Tremblay, M. Alducin, and J. I. Juaristi, Phys. Rev. Lett. **122**, 016806 (2019).
[12] Y. Huang, C. T. Rettner, D. J. Auerbach, and A. M. Wodtke, Science **290**, 111 (2000).
[13] B. C. Krüger, S. Meyer, A. Kandratsenka, A. M. Wodtke, and T. Schäfer, J. Phys. Chem. Lett. **7**, 441 (2016).
[14] R. J. V. Wagner, N. Henning, B. C. Krüger, G. B. Park, J. Altschäffel, A. Kandratsenka, A. M. Wodtke, and T. Schäfer, J. Phys. Chem. Lett. **8**, 4887 (2017).
[15] R. J. V. Wagner, B. C. Krüger, G. B. Park, M. Wallrabe, A. M. Wodtke, and T. Schäfer, Phys. Chem. Chem. Phys. **21**, 1650 (2019).

[16] N. Bartels, B. C. Kruger, D. J. Auerbach, A. M. Wodtke, and T. Schafer, Angew. Chem. Int. Ed. **53**, 13690 (2014).
[17] B. C. Kruger, N. Bartels, C. Bartels, A. Kandratsenka, J. C. Tully, A. M. Wodtke, and T. Schafer, J. Phys. Chem. C **119**, 3268 (2015).
[18] N. Bartels, K. Golibrzuch, C. Bartels, L. Chen, D. J. Auerbach, A. M. Wodtke, and T. Schafer, Proc. Natl. Acad. Sci. U.S.A. **110**, 17738 (2013).
[19] S. Li and H. Guo, J. Chem. Phys. **117**, 4499 (2002).
[20] R. Yin, Y. Zhang, and B. Jiang, J. Phys. Chem. Lett. **10**, 5969 (2019).
[21] R. Yin and B. Jiang, Phys. Rev. Lett. **126**, 156101 (2021).
[22] G. Meng, C. Hu, and B. Jiang, J. Phys. Chem. C **126**, 12003 (2022).
[23] C. L. Box, Y. Zhang, R. Yin, B. Jiang, and R. J. Maurer, JACS Au **1**, 164 (2021).
[24] Y. Zhang, C. L. Box, T. Schäfer, A. Kandratsenka, A. M. Wodtke, R. J. Maurer, and B. Jiang, Phys. Chem. Chem. Phys. **24**, 19753 (2022).
[25] N. Shenvi, S. Roy, and J. C. Tully, J. Chem. Phys. **130**, 174107 (2009).
[26] S. Monturet and P. Saalfrank, Phys. Rev. B **82**, 075404 (2010).
[27] W. Dou and J. E. Subotnik, J. Chem. Phys. **144**, 024116 (2016).
[28] T. Serwatka, G. Füchsel, and J. C. Tremblay, Phys. Chem. Chem. Phys. **22**, 6584 (2020).
[29] J. Gardner, D. Corken, S. M. Janke, S. Habershon, and R. J. Maurer, J. Chem. Phys. **158**, 064101 (2023).
[30] W. Dou and J. E. Subotnik, J. Phys. Chem. A **124**, 757 (2020).
[31] N. Shenvi and J. C. Tully, Faraday Discuss. **157**, 325 (2012).
[32] S. Roy, N. A. Shenvi, and J. C. Tully, J. Chem. Phys. **130**, 174716 (2009).
[33] N. Shenvi, S. Roy, and J. C. Tully, Science **326**, 829 (2009).
[34] R. Cooper, C. Bartels, A. Kandratsenka, I. Rahinov, N. Shenvi, K. Golibrzuch, Z. Li, D. J. Auerbach, J. C. Tully, and A. M. Wodtke, Angew. Chem. Int. Ed. **51**, 4954 (2012).
[35] K. Golibrzuch, P. R. Shirhatti, I. Rahinov, A. Kandratsenka, D. J. Auerbach, A. M. Wodtke, and C. Bartels, J. Chem. Phys. **140**, 044701 (2014).
[36] G. Meng and B. Jiang, J. Chem. Phys. **157**, 214103 (2022).
[37] M. Huang, X. Zhou, Y. Zhang, L. Zhou, M. Alducin, B. Jiang, and H. Guo, Phys. Rev. B **100**, 201407(R) (2019).
[38] D. M. Newns, Phys. Rev. **178**, 1123 (1969).
[39] J. C. Tully, J. Chem. Phys. **93**, 1061 (1990).
[40] See Supplemental Material at http://link.aps.org/supplemental/10.1103/PhysRevLett.133.036203 for details of computational methods and additional results, which includes Refs. [41–50].
[41] C. Hartwigsen, S. Goedecker, and J. Hutter, Phys. Rev. B **58**, 3641 (1998).
[42] Y. Zhang, J. Xia, and B. Jiang, J. Chem. Phys. **156**, 114801 (2022).
[43] B. Jiang and H. Guo, Phys. Chem. Chem. Phys. **16**, 24704 (2014).
[44] J. Xia, Y. Zhang, and B. Jiang, Chin. J. Chem. Phys. **34**, 695 (2021).
[45] J. C. Tully, J. Chem. Phys. **137**, 22A301 (2012).
[46] C. S. Pradhan and A. Jain, J. Chem. Theory Comput. **18**, 4615 (2022).
[47] X. Hu, W. L. Hase, and T. Pirraglia, J. Comput. Chem. **12**, 1041 (1991).
[48] W. L. Hase, *in Encyclopedia of Computational Chemistry*, edited by N. L. Alinger (Wiley, New York), pp. 399 (1998).
[49] M. C. Gutzwiller, *Chaos in Classical and Quantum Mechanics* (Springer, New York, 1990).
[50] Z. Jin and J. E. Subotnik, J. Chem. Phys. **150**, 164105 (2019).
[51] Q. Wu and T. Van Voorhis, Phys. Rev. A **72**, 024502 (2005).
[52] N. Holmberg and K. Laasonen, J. Chem. Theory Comput. **13**, 587 (2017).
[53] Y. Zhang, C. Hu, and B. Jiang, J. Phys. Chem. Lett. **10**, 4962 (2019).
[54] Y. Zhang, Q. Lin, and B. Jiang, WIREs Comput. Mol. Sci. **13**, e1645 (2023).
[55] T. D. Kühne *et al.*, J. Chem. Phys. **152**, 194103 (2020).
[56] M. Dion, H. Rydberg, E. Schröder, D. C. Langreth, and B. I. Lundqvist, Phys. Rev. Lett. **92**, 246401 (2004).
[57] P. R. Shirhatti, I. Rahinov, K. Golibrzuch, J. Werdecker, J. Geweke, J. Altschäffel, S. Kumar, D. J. Auerbach, C. Bartels, and A. M. Wodtke, Nat. Chem. **10**, 592 (2018).
[58] K. Golibrzuch, Ph.D. thesis, Georg-August-Universität Göttingen, 2014.
[59] K. Golibrzuch, P. R. Shirhatti, J. Altschaffel, I. Rahinov, D. J. Auerbach, A. M. Wodtke, and C. Bartels, J. Phys. Chem. A **117**, 8750 (2013).
[60] I. Lončarić, M. Alducin, J. I. Juaristi, and D. Novko, J. Phys. Chem. Lett. **10**, 1043 (2019).
[61] X. Zhou, G. Meng, H. Guo, and B. Jiang, J. Phys. Chem. Lett. **13**, 3450 (2022).
[62] G. Miao, W. Dou, and J. Subotnik, J. Chem. Phys. **147**, 224105 (2017).
[63] W. Dou and J. E. Subotnik, J. Chem. Phys. **148**, 230901 (2018).
[64] J. Gardner, S. Habershon, and R. J. Maurer, J. Phys. Chem. C **127**, 15257 (2023).
[65] P. K. De and A. Jain, J. Phys. Chem. A **127**, 4166 (2023).
[66] S. Malpathak and N. Ananth, J. Phys. Chem. Lett. **15**, 794 (2024).
[67] https://github.com/bjiangch/CO_Au111.
[68] J. Gardner, O. A. Douglas-Gallardo, W. G. Stark, J. Westermayr, S. M. Janke, S. Habershon, and R. J. Maurer, J. Chem. Phys. **156**, 174801 (2022).
[69] https://github.com/NQCD/NQCDynamics.jl.